25th ABCM International Congress of Mechanical Engineering
October 20-25, 2019, Uberlândia, MG, Brazil

COB-2019-1151
THE EFFECTS OF LATERAL-TORSIONAL COUPLING IN DRILL-STRING DYNAMICS

Lucas Passos Volpi
Daniel de Moraes Lobo
Thiago Gamboa Ritto
lp.volpi@mecanica.coppe.ufrj.br, daniel.lobo23@poli.ufrj.br,tritto@mecanica.ufrj.br

Universidade Federal do Rio de Janeiro, Department of Mechanical Engineering, Rio de Janeiro, Brazil

Abstract. *Drill-strings are subjected to a variety of vibrational phenomena that affects the drilling process and often leads to efficiency loss and even premature failure. These vibrations can be classified into axial, torsional and lateral. Although each dynamic can be modeled separately, the coupling between them can significantly affect the system response. In this paper, the effects of the coupling between lateral and torsional dynamics are discussed. The governing equations are obtained assuming a lumped parameter model for both lateral and torsional dynamics. The former considers the BHA an unbalanced rotor surrounded by a fluid with discontinuous impact with borehole wall. The latter models the drill-string as a torsional pendulum considering bit-rock interaction. Simulations regarding uncoupled and coupled dynamics shows that torsional vibrations governs the BHA lateral behavior and can induce lateral vibrations, while lateral vibrations may supress torsional vibrations.*

Keywords: *drill-string, lumped parameter model, stick-slip, whirling frequencies*

1. INTRODUCTION

Drilling operations are usually related to complex dynamical problems, specially regarding the drill-string vibration. A drill-string is a slender tubular structure that can be divided in two major sections: (i) the drill pipes, which composes most of drill-string length, and; (ii) the Bottom Hole Assembly (BHA), which is composed by a variety of equipments, including the drill-bit (Melakhessou *et al.*, 2003) . In order to drill the rock formation, an axial force (WOB) is applied on the rock surface by the bit, while a rotational motion is applied to the drill-string by the rotary table at the top of the drill-string. In order to mitigate lateral vibrations, the BHA is equipped with stabilizers throughout its extension, especially near the drill-bit.

Drill-strings are usually subjected to axial, torsional and lateral vibrations (Leine and Van Campen, 2002). These vibrations can cause the premature failure of the drill-string and, thus, studies regarding each of these phenomena are primordial to achieve a more efficient operation (Ghasemloonia *et al.*, 2014). These phenomena are commonly associated with highly non-linear problems and a simultaneous analysis of all three dynamics is very difficult (Al-Hiddabi *et al.*, 2003). Thus, each dynamic is typically approached individually (Yigit, 1998). In this work, the lateral-torsional dynamics is investigated.

The worst scenario in torsional vibration is commonly referred as 'stick-slip'. In this scenario, drill-bit can achieve rotational speeds that range from zero (stick) to 10 times the rotary table speed (slip). The cause of this phenomenon is usually attributed to the characteristics of the interaction between the bit and the rock formation (Lobo *et al.*, 2017).

In lateral vibration, the rotation axis that the drill-string rotates moves laterally in relation to the geometric center of the borehole. This motion is known as whirl and are commonly associated as a consequence of the eccentricity of the drill-string (Jansen, 1991; Kapitaniak *et al.*, 2017) and are classified accordingly to the rotation's direction. When the drill-string rotates around the borehole axis in the same direction as the rotary table, it is called forward whirl. Otherwise, when the whirl is in the opposite direction as the rotatory table, it is called backward whirl. The main cause of backward whirl is the contact between the drill-string and the borehole wall. Only the lowest portion of BHA works under compression, thus it is reasonable to assume that it is more susceptible to lateral vibration than the drill-pipes. Hence, studies regarding lateral vibrations are often restricted to the BHA region (Neubauer *et al.*, 2015).

The objective of this paper is to investigate the effects of the lateral-torsional coupling on the drill-string dynamics. The lateral dynamics is modeled as a Jeffcott rotor with fluid drag and discontinuous impact, while the torsional dynamics considers a torsional pendulum. The lateral-torsional coupling is included by means of the contact forces between the drill-string and borehole wall and by considering that the lateral stiffness depends on torsional effects. The results are

presented for both one-way and two-way couplings. A set of analysis regarding BHA rotation and whirl are conducted evaluating the effects of the coupling.

2. DRILL-STRING DYNAMIC MODEL

According to Jansen (1991), rotor-like behavior can be assumed for the lateral dynamics of drill-strings. The stabilizers in the BHA act as bearings, reducing the model to a simply supported shaft (Yigit, 1998). The torsional dynamics can be modeled by a torsional pendulum with the top rotating at a constant speed Ω, which is applied by the rotatory table. Figure 1 presents the drill-string with a schematic view of both torsional and lateral models.

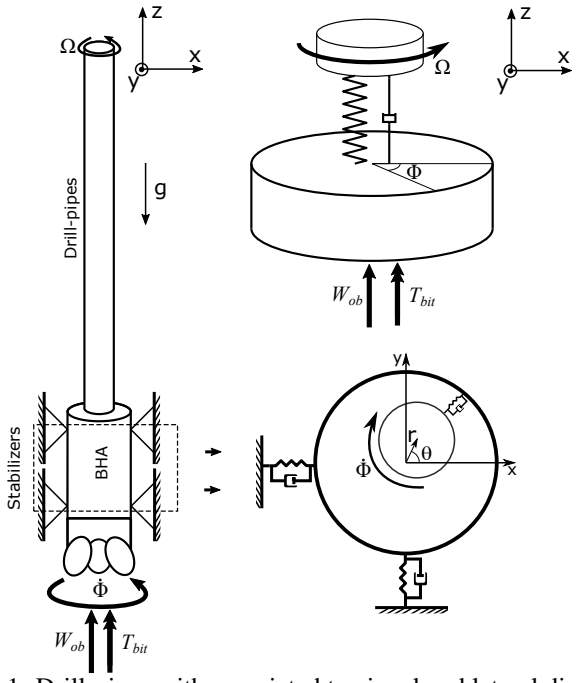

Figure 1: Drill-pipes with associated torsional and lateral diagrams.

As the drill-pipe is expressively longer than the BHA, it can be assumed that the BHA is rigid regarding torsional behavior (Lobo *et al.*, 2019). Thus, the system of equations of motion are:

$$\begin{aligned}
&m_t(\ddot{r} - \dot{\theta}^2 r) + c_h|\nu|\dot{r} + k(\dot{\phi})r = m_t g \sin\alpha\cos\theta + m_t e\dot{\phi}^2\cos(\phi-\theta) + m_t e\ddot{\phi}\sin(\phi-\theta) - \delta(r)F_n,\\
&m_t(\ddot{\theta}r + 2\dot{r}\dot{\theta}) + c_h|\nu|r\dot{\theta} = m_t g\sin\alpha\sin\theta + me\dot{\phi}^2\sin(\phi-\theta) - m_t e\ddot{\phi}\cos(\phi-\theta) - \delta(r)F_{fat},\\
&I_m\ddot{\phi} + k_t(\phi - \Omega t) + c_t(\dot{\phi} - \Omega) = -T_{bit} + T_{lat},
\end{aligned} \tag{1}$$

where r and θ are the BHA geometric center position; ϕ is the bit rotational angle; m_t is the total mass between the stabilizers, i.e. $m_t = m + m_f$, where m is the section mass and m_f is the fluid mass, found in Eqs. 2 and 3, respectively; I_m is the equivalent mass moment of inertia defined in Eq. 4; g is the gravity acceleration; k_t and c_t are the torsional stiffness and damping, respectively; e is the eccentricity; α is the wellbore inclination; c_h the hydraulic damping coefficient; $|\nu| = \sqrt{\dot{r}^2 + \dot{\theta}^2 r^2}$ is the modulus of BHA geometric center speed; $k(\dot{\phi})$ is the lateral stiffness, which depends on the bit rotational speed; The torques T_{bit} and T_{lat} describe the torque due to bit-rock interaction and the torque due to coupling to lateral dynamics. Finally, δ defines the Heaviside function, where $\delta = 1$ if $r \geq r_c$ and $\delta = 0$ if $r < r_c$, considering r_c as the radial clearance between the BHA and the borehole wall.

$$m = \frac{\pi\rho(D_{co}^2 - D_{ci}^2)L_c}{8}, \tag{2}$$

$$m_f = \frac{\pi\rho_f(D_{ci}^2 + C_A D_{co}^2)L_c}{8} \tag{3}$$

and

$$I_m = I_b + \frac{1}{3} I_p, \tag{4}$$

where D_{ci}, D_{co} and L_c as the outer diameter, inner diameter and length of the BHA section, respectively; C_A is the added fluid mass coefficient; I_b and I_p are the mass moment of inertia of the BHA and drill-pipes, respectively;

The lateral stiffness accounts for the effects of a constant axial force and a variable torque on bit. According to Yigit (1998), the axial load and torque can be approximated by the W_{ob} and T_{bit}, respectively:

$$k(\dot{\phi}) = \frac{E I_a \pi^4}{2 L_c^3} - \frac{T_{bit}(\dot{\phi}) \pi^3}{2 L_c^2} - \frac{W_{ob} \pi^2}{2 L_c}, \tag{5}$$

where $I_a = \rho(D_{co}^4 - D_{ci}^4)/64$ is the area moment of inertia of the BHA. The contact between the drill-string and the borehole wall is modeled by a discontinuous elastic force (Jansen, 1991) in the presence of Coulomb friction. In order to regularize the friction model, the model used by Divenyi *et al.* (2006) is adopted:

$$F_n = k_s (r - r_c), \tag{6}$$

$$F_{at} = \mu \tanh\left(v_{rel}/V_{ref}\right) F_n, \tag{7}$$

where k_s is the contact stiffness; $v_{rel} = \dot{\phi} R_{co} + \dot{\theta} r$ describes the relative velocity during contact (Moraes and Savi, 2018), where R_{co} is the BHA radius, and; V_{ref} is a constant. The torque on bit is modeled according to Tucker and Wang (1997):

$$T_{bit} = W_{ob} b_0 \left(\tanh\left(b_1 \dot{\phi}\right) + \frac{b_2 \dot{\phi}}{1 + b_3 \dot{\phi}^2} \right), \tag{8}$$

where b_0, b_1, b_2 and b_3 are constants of the bit-rock interaction model. Finally, the torque due to the lateral dynamics are defined as (Yigit, 1998):

$$T_{lat} = -c_v |\nu| \left[\dot{r} e \sin\left(\phi - \theta\right) - r \dot{\theta} e \cos\left(\phi - \theta\right) \right] - \delta(r) F_n e \sin\left(\phi - \theta\right) - \delta(r) F_{fat} \left(R_{co} - e \cos\left(\phi - \theta\right) \right). \tag{9}$$

3. RESULTS

The equations of motion are solved using the 5th-order Runge-Kutta method. In order to guarantee the convergence in the integration during discontinuities, a time step of the order of $\Delta t \approx 10^{-5}$ s is used. In addition, whenever the dynamic crossed the discontinuity point, the absolute error was calculated according to Eq. 10. If the error crossed a threshold of $err > 0.001$, the time step is reduced by half, in order to guarantee that the discontinuity point is not overstepped.

$$err = \frac{|r - r_c|}{r_c} \tag{10}$$

The parameters assumed in this work are depicted in Tab. 1 and they are in accordance with the drill-string analyzed by Ritto *et al.* (2017). The drill-string is considered nearly vertical, i.e. $\alpha \approx 0$, with approximately 5000 m of length. The lateral dynamics is simulated for a BHA section with 8.55 m between stabilizers.

Table 1: Summary of drill-string properties

Parameter	Symbol	Values	Units	Parameter	Symbol	Values	Units
Young's Modulus	E	220	GPa	Viscous damping	c_h	465.39	Ns^2/m^2
Total mass	m_t	909.52	kg	Torsional stiffness	k_t	314.56	kg m/s^2
Eccentricity	e	1.4	mm	Torsional damping	c_t	178.21	kg m/s
Contact stiffness	k_s	10^9	N/m	Area inertia	I_a	4.07×10^{-5}	m^4
Equivalent inertia	I_m	455.24	kg m^2	Friction constant	V_{ref}	1×10^{-4}	m/s
Wall friction coeff.	μ	0.35	-	T_{bit} model constant	b_0	2.39×10^{-12}	-
Wellbore inclination	α	10^{-7}	rad	T_{bit} model constant	b_1	1.91	s
Gravity	g	9.81	m/s^2	T_{bit} model constant	b_2	8.50	s
Length of BHA section	L_c	8.55	m	T_{bit} model constant	b_3	5.47	s^2
BHA inner diameter	D_{ci}	0.071	m	Added mass coefficient	C_A	1.7	
BHA outer diameter	D_{co}	0.171	m				

In Fig. 2, the system response is analyzed for the two-way coupled case and for the one-way coupled case, which considers the coupling in lateral dynamics but not in torsional dynamics, i.e. $T_{lat} = 0$ kNm. Figures 2a and 2b presents five distinct curves for the bit rotational speed. The W_{ob} of 220 kN induces severe torsional vibrations in the uncoupled model. However, it can be noticed that the torsional-lateral coupling leads to a different behavior, whereas the torques generated by lateral impact resists torsional vibrations and might interrupt the severe torsional vibration. A lower W_{ob} does not present meaningful torsional vibrations, as expected. Figures 2c and 2d presents the displacement of the geometric center of BHA section due to the whirling motion. In the case with severe torsional vibrations (case 2), there is a periodic collision motion due to the rotational speed peaks in slip phase. Without severe torsional vibrations, the BHA remains near the borehole wall, with exception of case 5, where the BHA returns to oscillate near the resting region due two smaller peaks in the transient in torsional vibrations. The non-linearity in the fluid damping model also implies in longer transient stages in lower speeds (cases 4 and 5).

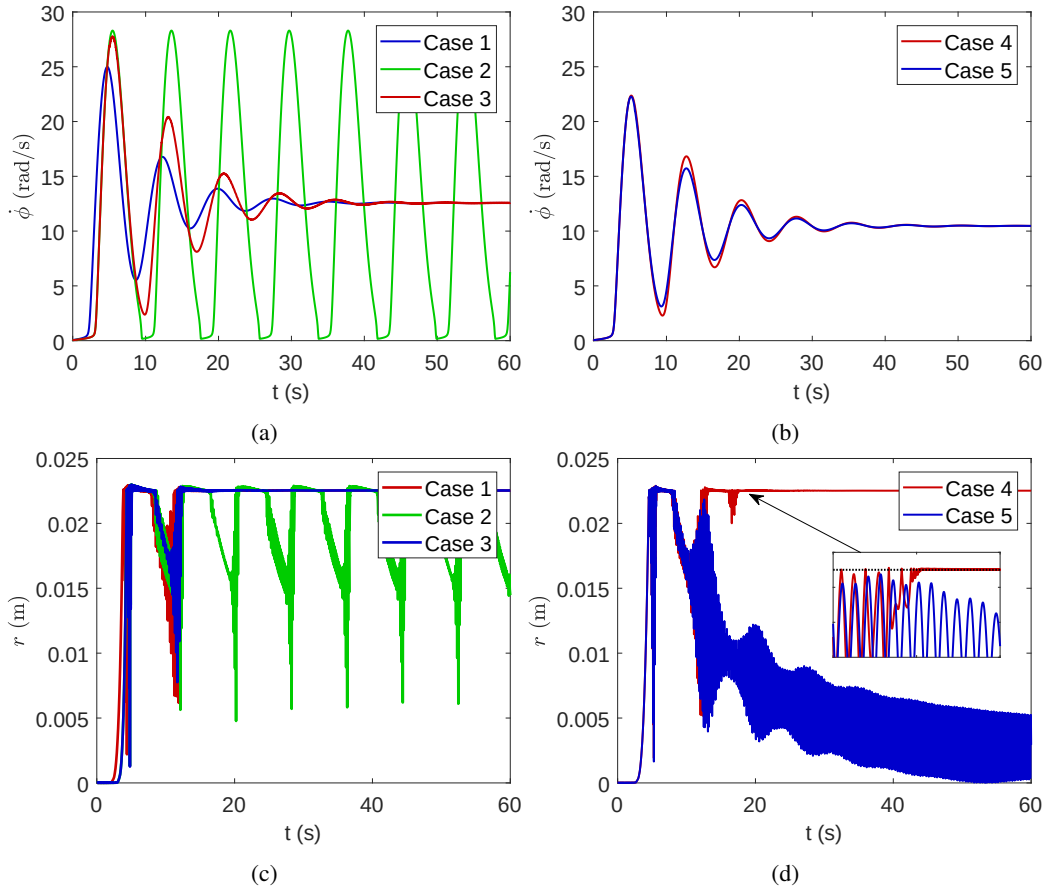

Figure 2: (a) BHA rotational speed where $\Omega = 12.57$ rad/s, (b) BHA rotational speed where $\Omega = 10.47$ rad/s, (c) and (d) are BHA radial displacement. Case 1: 1-way coupled ($W_{ob} = 160$ kN); Case 2: 1-way coupled ($W_{ob} = 220$ kN); Case 3: 2-way coupled ($W_{ob} = 220$ kN); Case 4: 1-way coupled ($W_{ob} = 160$ kN); Case 5: 2-way coupled ($W_{ob} = 160$ kN)

Figure 3 presents the orbit of the BHA in the steady state for cases 2 through 5. In Fig. 3a, there is a clear impact regimen, with the BHA colliding with the borehole wall and returning. A consequence is a high variation in the BHA position. Figures 3b and 3c presents a steady contact with the wall, implying in an orderly contact configuration and a backward whirl regime, as it shown in sequence. However, in Fig. 3d, it is clear that the BHA does not collide in the steady state, and hence, is a contact-less forward whirl regimen.

Figure 4 depicts the BHA whirling speed throughout time for uncoupled and coupled cases by using the spectrogram. In order to generate each spectrogram, it was re-written in complex polar coordinates (Tiwari, 2017):

$$z = x + iy, \tag{11}$$

where $x = r\cos\theta$; $y = r\sin\theta$ and i is the imaginary unit $i = \sqrt{-1}$. Hence, it can be re-written as:

$$z = r(\cos\theta + i\sin\theta) \quad \text{or} \quad z = re^{i\theta}. \tag{12}$$

The spectrogram was then generated to evaluate the variable z. As $z \in \mathbb{C}$, a Fast Fourier Transform provided an asymmetric frequency spectrum. This procedure provides negative values for frequencies, each representing a backward

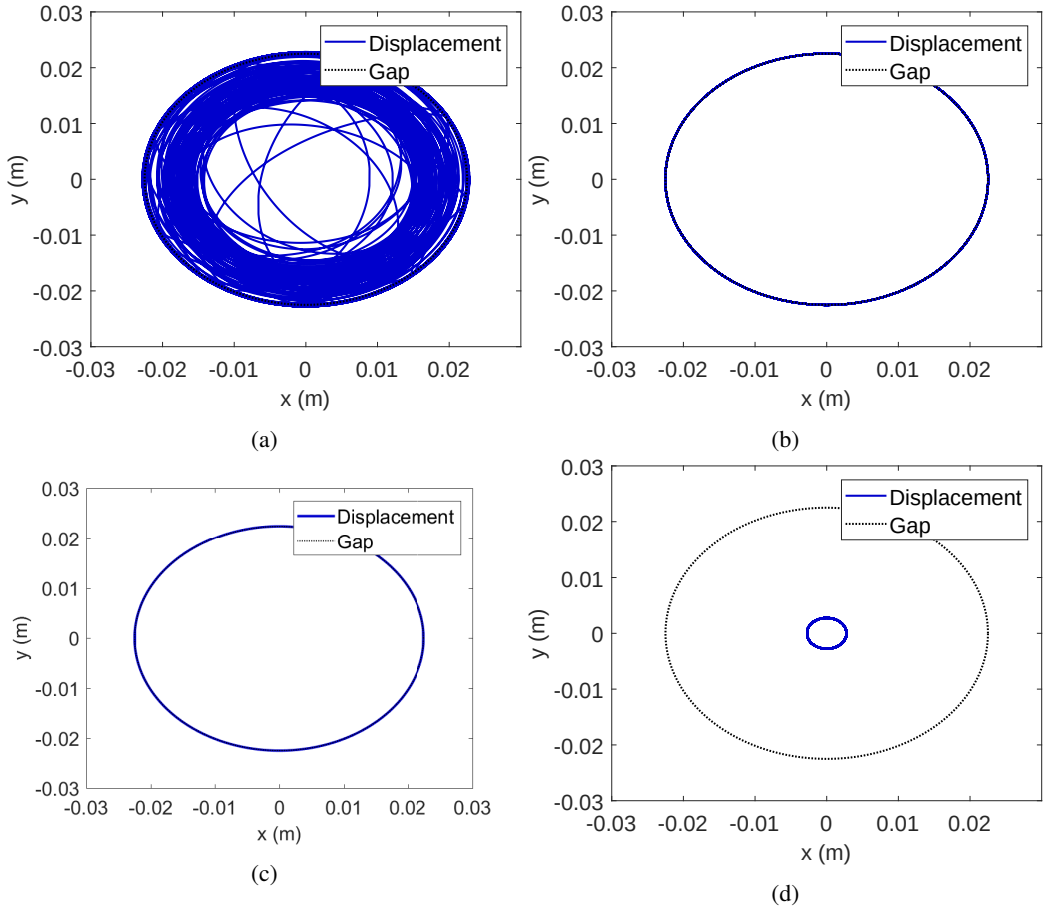

Figure 3: BHA geometric center orbit in the steady state with: (a) 1-way coupled ($W_{ob} = 220$ kN and $\Omega = 12.57$ rad/s); (b) 2-way coupled model ($W_{ob} = 220$ kN and $\Omega = 12.57$ rad/s); (c) 1-way coupled ($W_{ob} = 160$ kN and $\Omega = 10.47$ rad/s); (d) 2-way coupled model ($W_{ob} = 160$ kN and $\Omega = 10.47$ rad/s).

whirl frequency, while positive values refer to forward whirl frequency. The same procedure was adopted to generate the spectrogram, which consists in 1024 windows and sample frequency of 10^5 Hz.

In Fig. 4a (with $\Omega = 12.57$ rads and $W_{ob} = 220$ kN), it can be noticed that, during slip phase, the whirling speed reaches negative values. In other words, the BHA is in a backward whirling motion. During stick, it vibrates near the first lateral natural frequency defined by Eq. 13 : $\omega_{n1} = 3.89$ Hz. In Fig. 4b, 2-way coupling is considered with similar operation conditions. As this coupled condition prevents severe torsional vibration, the BHA behaves in a rotor-like dynamic, with whirl frequency in accordance with the drill-string rolling speed presented in Eq. 14 (Minett-Smith *et al.*, 2010), thus, it presents a backward whirl frequency of: $\omega_{bw} = -7.60$ Hz.

$$\omega_{n1}(\dot{\phi}(t)) = [k(\dot{\phi}(t))/m_t]^{\frac{1}{2}}; \tag{13}$$

$$\omega_{bw} = -\frac{R\dot{\phi}}{r_c}. \tag{14}$$

In Fig. 4c, once more, a backward whirl configuration can be found for the 1-way coupled model with $\Omega = 10.47$ rads and $W_{ob} = 160$ kN. The full coupling in Fig. 4d presents a forward whirl dynamic for the same Ω and W_{ob} configuration. This contrast in regimen could be explained by the difference of amplitude in torsional speed between models during the transient phase. As a consequence, the second torsional speed peak in case 4 is enough to cause the impact and rolling of the BHA, which accelerates the whirl and increases the centripetal force component in Eq. 1. This leads to enough radial displacement to configure contact and a backward whirl regime, which obeys the rolling condition, with $\omega_{bw} = -6.33$ Hz. This particularity does not occur after the first impact because, even though the whirling speed is high, the torsional speed decreases enough to prevent continuous contact.

4. CONCLUSION

A theoretical analysis is presented regarding the effects of the lateral-torsional coupling in drill-string vibrations. A non-linear, discontinuous, lumped parameter model is used for both coupled and uncoupled dynamics and the equations

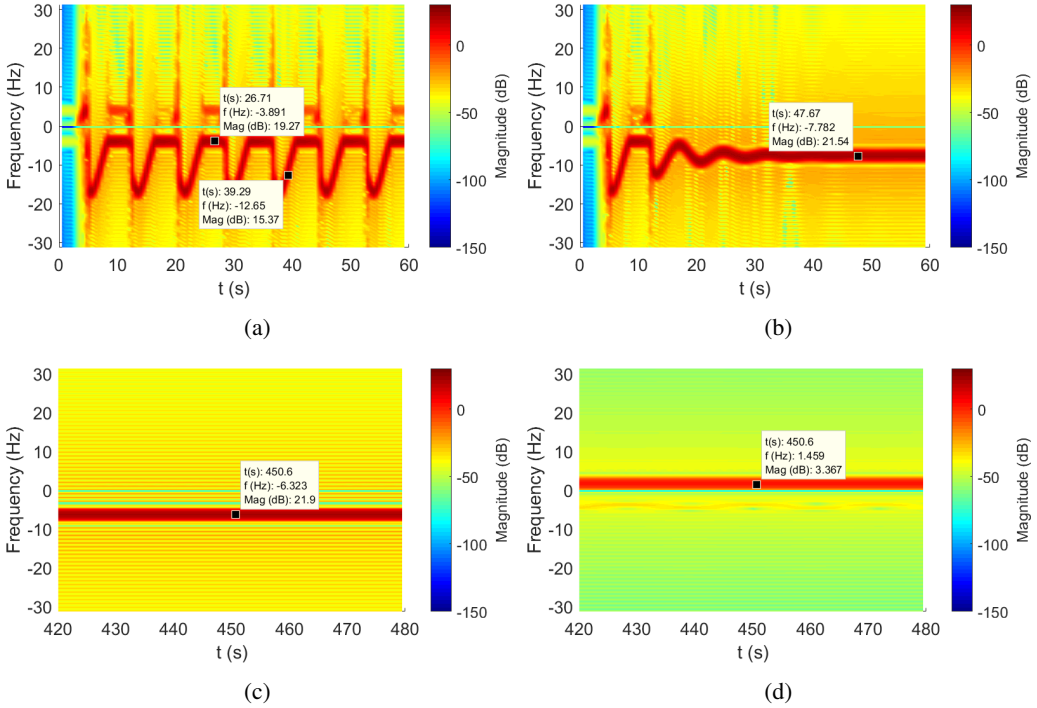

Figure 4: whirl frequency development through time for: (a) 1-way coupled ($W_{ob} = 220$ kN and $\Omega = 12.57$ rad/s); (b) 2-way coupled model ($W_{ob} = 220$ kN and $\Omega = 12.57$ rad/s); (c) 1-way coupled ($W_{ob} = 160$ kN and $\Omega = 10.47$ rad/s); (d) 2-way coupled model ($W_{ob} = 160$ kN and $\Omega = 10.47$ rad/s).

are numerically solved. A comparison between the models showed that the lateral motion can be responsible for reducing torsional vibrations. However, in the presence of severe torsional oscillations, the coupling results in a lateral vibration that is strongly dependent on the rotational speed, and hence, torsional vibration can induce a collision regimen with borehole wall for certain values of W_{ob}. The combination of phenomena of both severe torsional and lateral vibration is highly critical to the BHA and can lead to fatigue and premature failure, in other words, severe torsional vibrations with the existence of backward whirl can jeopardize de drilling process.

The presence of torques due to lateral motion is also a key component in the system's dynamics. The 2-way coupling does not only affects torsional vibrations, as expected, but can also significantly change lateral dynamics. Those torques can resist the torsional vibrations and, in some cases, even stabilize the torsional system. Meanwhile, small changes in torsional speed behavior can affect lateral vibrations as high amplitudes, even with torsional speeds converging to a similar value in steady state, can lead to the contact of the BHA with borehole and even a rolling motion. Hence, the mitigation of torsional vibrations can induce the reduction of lateral vibrations, which increases the efficiency of the drilling process.

5. ACKNOWLEDGEMENTS

This study was financed in part by the Coordenacao Aperfeicoamento de Pessoal de Nıvel Superior (CAPES) - Finance code 001 - Grant PROEX 803/2018, and the Brazilian agencies: Conselho Nacional de Desenvolvimento Cientıfico e Tecnologico (CNPQ) - Grants 303302/2015-1, 400933/2016-0, Fundacao Carlos Chagas Filho de Amparo a Pesquisa do Estado do Rio de Janeiro (FAPERJ) - Grant E-26/201.572/2014.

6. REFERENCES

Al-Hiddabi, S.A., Samanta, B. and Seibi, A., 2003. "Non-linear control of torsional and bending vibrations of oilwell drillstrings". *Journal of Sound and Vibration*, Vol. 265, No. 2, pp. 401–415. ISSN 0022460X. doi:10.1016/S0022-460X(02)01456-6.

Divenyi, S., Savi, M.a., Franca, L.F.P. and Weber, H.I., 2006. "Nonlinear dynamics and chaos in systems with discontinuous support". *Shock and Vibration*, Vol. 13, No. 4-5, pp. 315–326. ISSN 1070-9622.

Ghasemloonia, A., Geoff Rideout, D. and Butt, S.D., 2014. "Analysis of multi-mode nonlinear coupled axial-transverse drillstring vibration in vibration assisted rotary drilling". *Journal of Petroleum Science and Engineering*, Vol. 116, pp. 36–49. ISSN 09204105. doi:10.1016/j.petrol.2014.02.014.

Jansen, J., 1991. "Non-linear rotor dynamics as applied to oilwell drillstring vibrations". *Journal of sound and vibration*,

Vol. 147, No. 1, pp. 115–135.

Kapitaniak, M., Vaziri, V., Paéz Chávez, J. and Wiercigroch, M., 2017. "Numerical Study of Forward and Backward Whirling of Drill-String". *J. Comput. Nonlinear Dynam.*, Vol. 12, No. 6, pp. 1–7. ISSN 15551423.

Leine, R.I. and Van Campen, D.H., 2002. "Stick-slip whirl interaction in drillstring dynamics". *Journal of Vibration and Acoustics*, Vol. 122, No. April, pp. 287–296. ISSN 09250042.

Lobo, D.M., Ritto, T.G. and Castello, D.A., 2017. "Stochastic analysis of torsional drill-string vibrations considering the passage from a soft to a harder rock layer". *Journal of the Brazilian Society of Mechanical Sciences and Engineering*, Vol. 39, No. 6, pp. 2341–2349. ISSN 1678-5878.

Lobo, D.D.M., Ritto, T.G. and Massa, F.D., 2019. "A comparison between modeling strategies for the torsional dynamics of drill-strings using lumped-parameter models". In *Proceedings of the 25th International Congress of Mechanical Engineering - COBEM 2019*.

Melakhessou, H., Berlioz, A. and Ferraris, G., 2003. "A Nonlinear Well-Drillstring Interaction Model". *Journal of Vibration and Acoustics*, Vol. 125, No. 1, p. 46. ISSN 07393717. doi:10.1115/1.1523071.

Minett-Smith, D.J., Stroud, D.R.H. and Pagett, J.M., 2010. "Real-Time Whirl Detector Aids Drilling Optimization". *SPE Annual Technical Conference and Exhibition*, , No. SPE 135110, pp. 1–18. ISSN 1070-664X. doi:10.2118/135110-MS.

Moraes, L.P.P.D. and Savi, M.A., 2018. "Drill-String Vibration Analysis Considering an Axial-Torsional-". *Journal of Sound and Vibration*, Vol. 438, pp. 220–237. ISSN 0022-460X.

Neubauer, M., Ilja, G. and Jorg, W., 2015. "Model and Method for a Time-Efficient Analysis of Lateral Drillstring Dynamics". In ASME GT2015, ed., *ASME Turbo Expo 2015: Turbine Technical Conference and Exposition GT2015*. Montréal, pp. 1–13.

Ritto, T., Aguiar, R. and Hbaieb, S., 2017. "Validation of a drill string dynamical model and torsional stability". *Meccanica*, Vol. 52, No. 11-12, pp. 2959–2967.

Tiwari, R., 2017. *Rotor systems: analysis and identification*. CRC Press.

Tucker, R.W. and Wang, C., 1997. "The Excitation and Control of Torsional Slip-Stick In the Presence of Axial-Vibrations". pp. 1–5.

Yigit, A.S. e Christoforou, A., 1998. "Coupled torsional and bending vibrations of drillstrings subject to impact with friction". *Journal of Sound and Vibration*, Vol. 215, No. 1, pp. 167–181.